Chapter-4

Metal Dusting Behavior of Fe-18Cr-21Mn-0.65N Austenitic Stainless Steel

4.1. Introduction

Austenitic stainless steels are used as a barrier layer coating against high temperature oxidation and corrosion in petrochemical industries and refineries. Stainless steels in form of pipes/ tubes are also used for the transport of process gas, carrying mixtures of CO and H_2. In metal dusting, metal/alloy surface disintegrates in form of dust, in the presence of reducing atmosphere (CO and H_2). During this, the type of oxide layer formed on the surface plays a very important role. Alloys capable of forming chromia and alumina layers possess good resistance against metal dusting for certain time intervals [106, 107]. In such cases, metal dusting starts from the defects present on the oxide layer and cracks generated due to localized rupture of protective scale. At low temperature (<500°C), the oxide layer does not form fully on the surface due to low diffusivity of matrix elements. Chun et al. [108] showed that in higher chromium containing steels (>9wt% Cr), oxide layer rupture causes direct migration of carbon and carbides form near the surface region, and their volume expansion results in disintegration of the surface. Manganese exhibits anti coking property and inhibits diffusion of carbon into the steel matrix. A study carried out on $MnCr_2O_4$ and Cr_2O_3 spinel in metal dusting environment showed that $MnCr_2O_4$ exhibited better resistance compared to Cr_2O_3 layer in the carburizing environment [109]. This chapter encompasses a systematic investigation to understand the features of metal dusting process of a high Mn austenitic stainless steel (with extremely low nickel) in syngas environment (25 %CO and 75%H_2) from 400-700°C, under cyclic exposure for 300 h. Carbon corrosion occurred at 400-500°C, however, at 600-700°C, oxidation of Mn and formation of Mn-Cr-O spinel significantly reduced the carbon corrosion. The surface and cross section of the exposed coupons were examined by XRD, SEM(EDS) and EPMA. Metal dusting resulted in formation of very few corrosion pits of the size 2-7µm and epitaxial growth of carbon nanotubes on the surface exposed at 400-500°C.

4.2. Results

4.2.1 Visual Observation and Weight Gain Analysis

Carbon deposition was not significant on the samples exposed up to 100 h at all the temperatures of exposure (< 1mg/cm^2). Therefore, the time of exposure was increased to 300 h for all the temperatures of exposure. **Figure 4.1** shows that at 400 to 500°C, carbon deposition (black color) was maximum while at 600 to 700°C, it was minimum. High carbon activity resulted in higher and discontinuous carbon deposition. The net weight gain of carbon with the time of exposure is shown in **Figure 4.2 a.** The weight gain of carbon was 0.41, 1.21, 1.65 and 1.92 mg/cm^2 at 400, 500, 600 and 700°C respectively. The net carbon deposited in each case is shown in **Figure 4.2 a**, it shows that at 400 and 500°C carbon deposition was highest (0.35-0.45 mg/cm^2) whereas at 600 and 700°C it was minimum (<0.2 mg/cm^2).

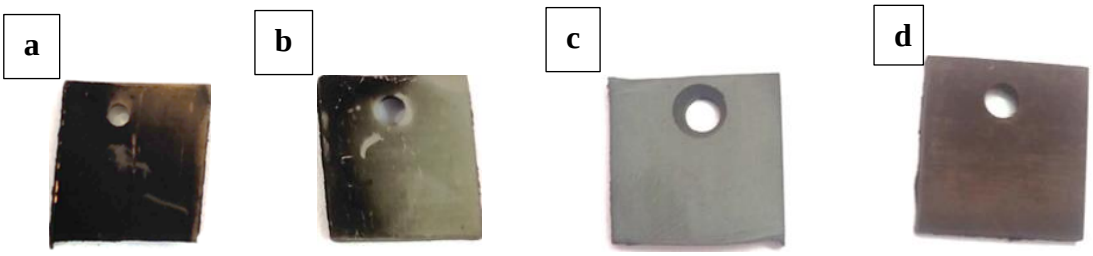

Figure 4.1: Photographs of metal dusted coupons exposed for 300 h at (a) 400°C, (b) 500°C, (c) 600°C and (d) 700°C.

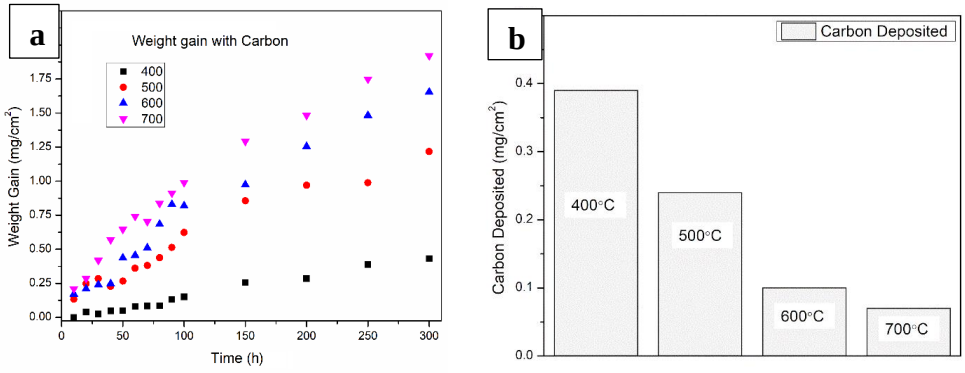

Figure 4.2: Plots, resulting from exposure of 300 h (a) weight gain vs time and (b) carbon deposited with respect to temperature.

4.2.2 XRD Analysis

X-ray diffraction patterns of metal dusted coupons exposed at 400-700°C are shown in **Figure 4.3 a** and the phases formed on the metal dusted coupons from the above exposures,

were characterized as MnO, Mn_3O_4, $FeMn_2O_4$, $MnCr_2O_4$, Mn_3C_7, and Fe_3C (Table 4.1). At 400 and 500°C, Mn oxide formation resulted in destabilization of the austenite matrix and formation of ferrite peaks was observed. The most prominent phase formed at 600 and 700°C was MnO. It seems to be the most stable oxide in the present carbonaceous/ reducing environment. Spinel such as $FeMn_2O_4$ and $MnCr_2O_4$ also formed at 600 and 700°C. Carbide precipitation shows ingression of carbon into the metal surface and peaks get stronger with increasing temperature.

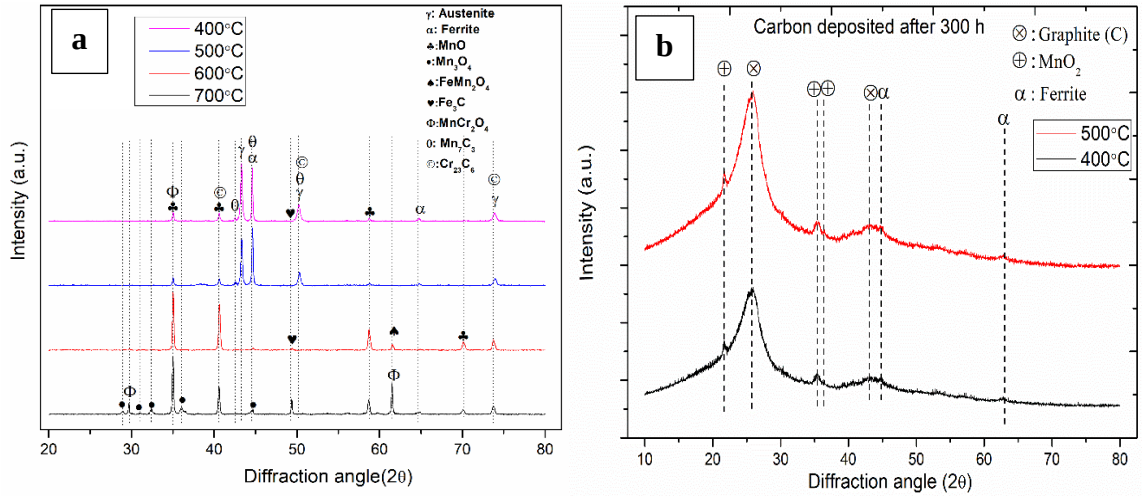

Figure 4.3: XRD patterns of (a) metal dusted coupons exposed at 400°C, 500°C, 600°C, and 700°C (b) carbon deposited at the surface from 300 h of exposure at 400°C and 500°C.

Table 4.1: Phases identified by XRD analysis after metal dusting process at different temperatures.

Temperature (°C)	Phases formed
400	γ, α, Mn_7C_3, $Cr_{23}C_6$, MnO, $MnCr_2O_4$
500	γ, α, Mn_7C_3, $Cr_{23}C_6$, MnO, $MnCr_2O_4$
600	γ, α, MnO, $MnCr_2O_4$, $FeMn_2O_4$, Fe_3C, $Cr_{23}C_6$
700	γ, α, MnO, $MnCr_2O_4$, $FeMn_2O_4$, Fe_3C, $Cr_{23}C_6$, Mn_3O_4

XRD analysis of the carbon (**Figure 4.3 b**), deposited on the surface of the coupons exposed at 400 and 500°C for 300 h, shows that carbon was present in the form of graphite. It reveals that iron/ferrite dust along with MnO_2 was also present.

4.2.3 Surface Morphology

The surfaces of the metal dusted coupons were thoroughly examined under SEM and the following observations were made.

Exposure at 400°C

Surface morphologies of the metal dusted coupon exposed at 400°C for 300 h are shown in **Figure 4.4**. It can be seen that deposition of carbon was not uniform throughout the surface. SEM images from different regions of the metal dusted coupon show different morphologies. **Figure 4.4 a** shows heavy deposition of carbon, the high magnification image (**Figure 4.4 c**) shows that carbon deposited at the surface is filamentous. EDS analysis at spots

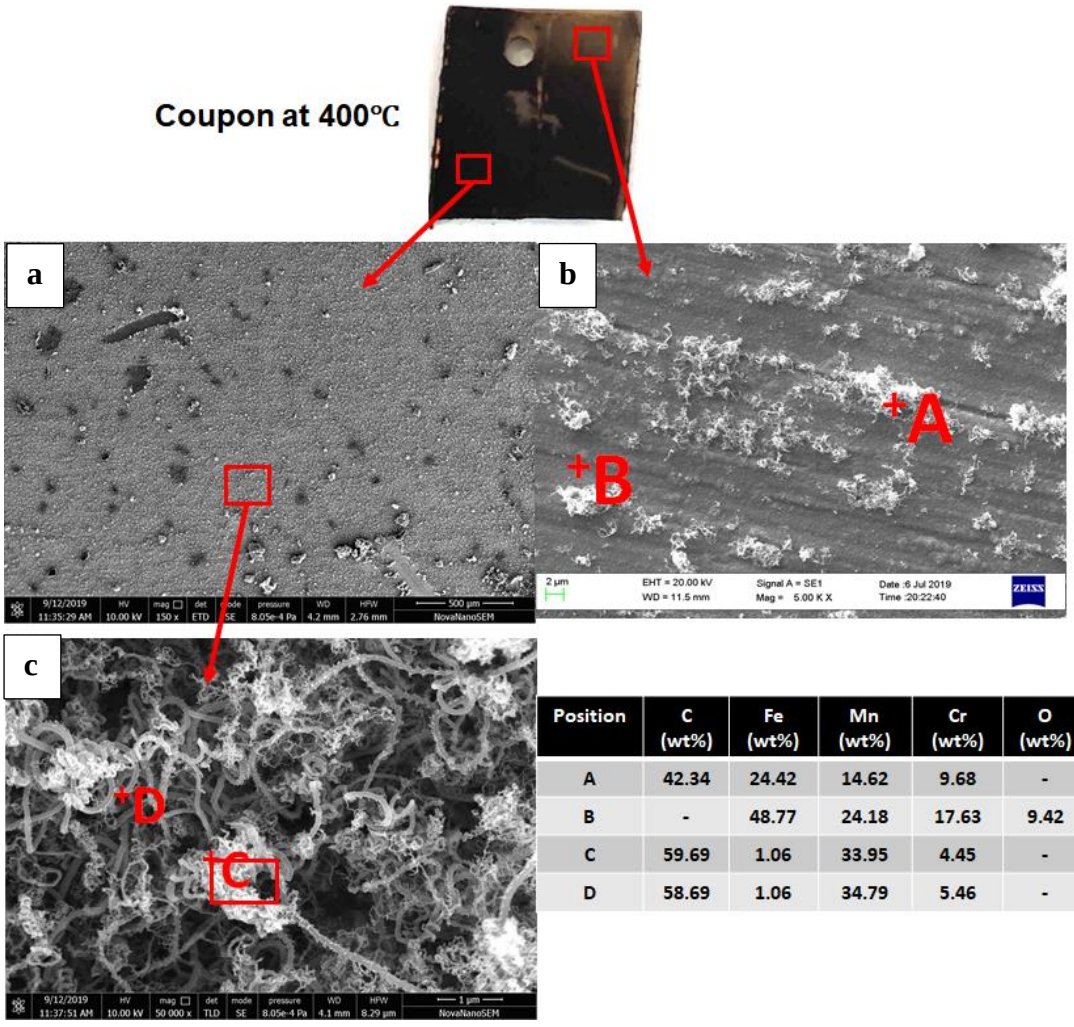

Position	C (wt%)	Fe (wt%)	Mn (wt%)	Cr (wt%)	O (wt%)
A	42.34	24.42	14.62	9.68	-
B	-	48.77	24.18	17.63	9.42
C	59.69	1.06	33.95	4.45	-
D	58.69	1.06	34.79	5.46	-

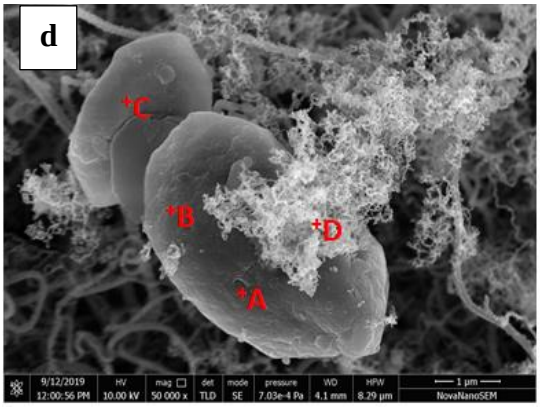

Position	Cr (Wt%)	Fe (Wt%)	Mn (Wt%)	C (wt%)
A	13.60	1.54	24.43	60.43
B	12.92	2.88	21.68	62.52
C	11.13	1.07	17.67	70.12
D	5.50	5.19	23.01	66.30

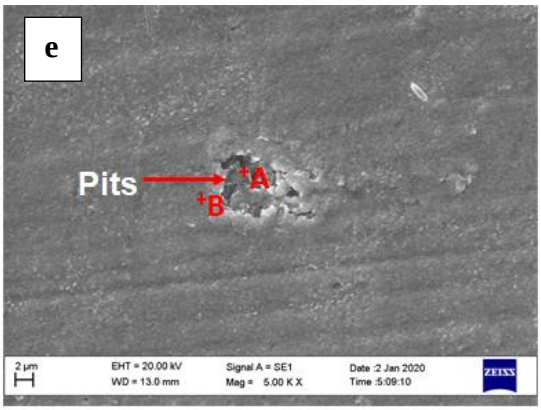

Position	C (wt%)	Cr (wt%)	Mn (wt%)	Fe (wt%)	O (wt%)
A	19.36	10.70	22.47	25.62	21.85
B	-	-	38.94	30.50	30.56

Figure 4.4: SEM micrographs and corresponding EDS of (a) carbon deposited region; (b) area of less deposition of carbon; (c) carbon filaments showing branched structure; (d) fragmented particle and (e) pits formation at the surface after carbon removal on metal dusted coupon exposed at 400°C for 300 h.

C and D of carbon filament (**Figure 4.4 c**) shows a higher amount of manganese, in line with XRD analysis of the carbon powder. Other matrix elements such as Fe and Cr were also present but in less quantity. SEM micrograph of spot A (**Figure 4.4 b**) in the region where carbon deposition was less shows that growth of carbon filaments was in a scattered manner. EDS analysis of spot B (**Figure 4.4 b**) reveals presence of oxygen with other alloying elements. Oxide formation may be due to water dissociation (reaction 1.12).

Figure 4.4 d shows SEM image of an elliptical metal particle, detached from the metal matrix. These particles also acted as catalyst sites for nucleation and growth of fine carbon filaments. EDS of the particles (**Figure 4.4 d** spots A, B, and C) shows a high content of carbon with some manganese and chromium in it. It could be supersaturated carbide of manganese and other elements which get detached from the metal surface after volume

expansion. SEM image of the surface after carbon removal by ultrasonic cleaning shows a pit of irregular size (**Figure 4.4 e**). At the center of the pits (**Figure 4.4 e**, spot A), carbon was observed with matrix elements. EDS analysis around the pits showed a spinel layer of Mn-Cr-Fe-O.

Exposure at 500°C

Figure 4.5 shows SEM micrograph of the metal dusted coupon exposed at 500°C for 300 h. Carbon deposition was less as compared to that at 400°C and had globular morphology (**Figure 4.5 c**). Pits were also present on the exposed surface. Carbon deposition was predominantly non-uniform, as shown in **Figure 4.5 a**. EDS analysis of spot C (**Figure 4.5 c**) shows that manganese was present with carbon. EDS analysis at the tip of the filaments (**Figure 4.5 c**, spot E) reveals presence of iron in very less quantity while EDS analysis of the middle part of the filament (**Figure 4.5 c**, spot D) shows traces of iron and manganese.

The SEM micrograph (**Figure 4.5 b**) from the area where carbon was deposited in less quantity shows globular shape (**Figure 4.5 b**, spot A), and spider web type of network containing Mn, Fe, Cr, C and O. **Figure 4.5 b** (spot B) shows oxide layer composed of spinel of Fe-Cr-Mn-O. The growth of globules occurred in a very localized fashion. **Figure 4.5 d** shows a pit formed on the surface after carbon removal. EDS analysis at the bottom of the pit (**Figure 4.5 d** spot A) shows the elements Fe, Mn, Cr along with some amount of carbon and oxygen. It clearly shows internal carburization of the matrix elements. The top surface around the pit (**Figure 4.5 d** spot B), composed of Fe, Cr, Mn, and O, confirmed the formation of spinel, observed from the XRD analysis.

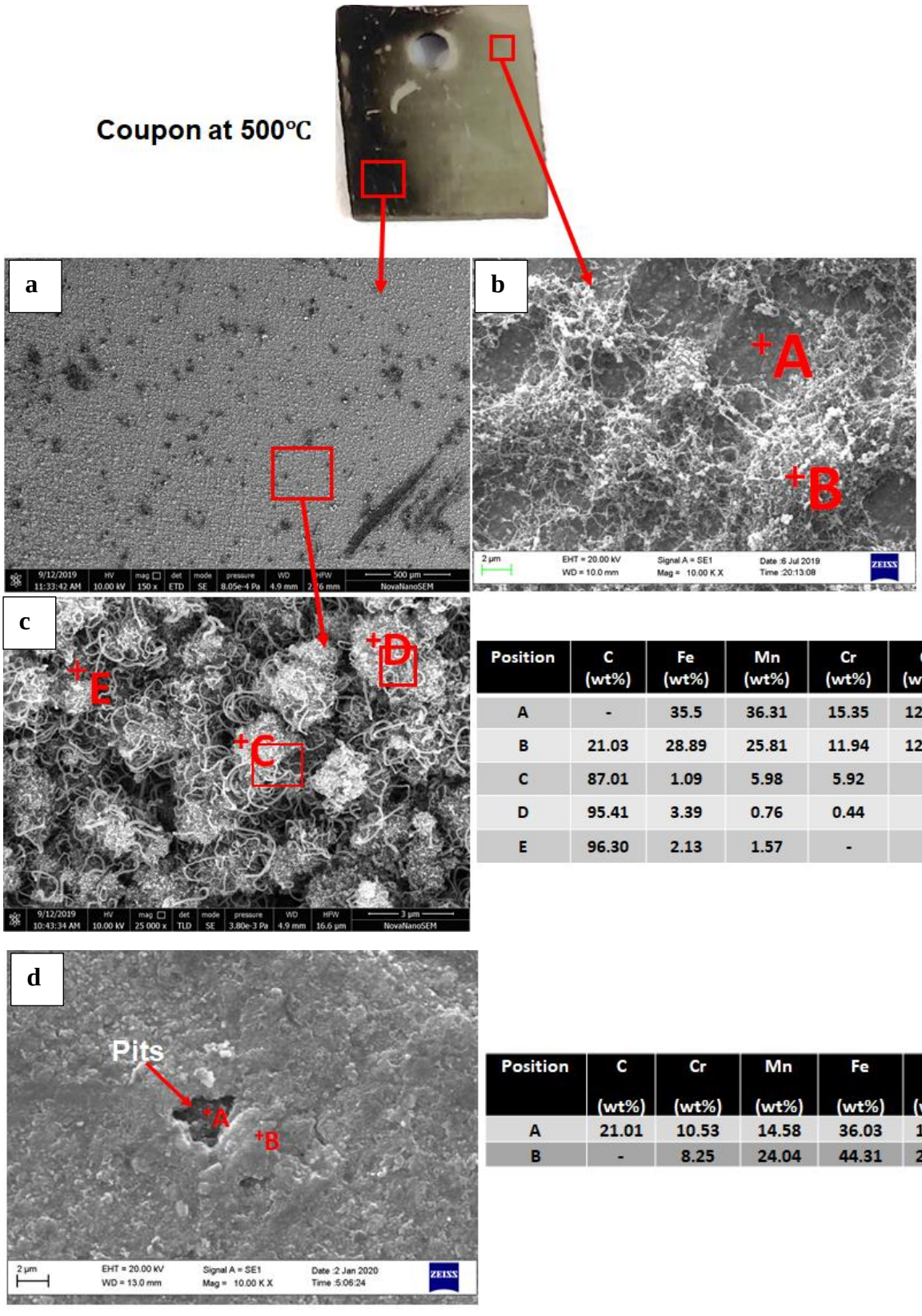

Position	C (wt%)	Fe (wt%)	Mn (wt%)	Cr (wt%)	O (wt%)
A	-	35.5	36.31	15.35	12.84
B	21.03	28.89	25.81	11.94	12.33
C	87.01	1.09	5.98	5.92	-
D	95.41	3.39	0.76	0.44	-
E	96.30	2.13	1.57	-	-

Position	C (wt%)	Cr (wt%)	Mn (wt%)	Fe (wt%)	O (wt%)
A	21.01	10.53	14.58	36.03	17.85
B	-	8.25	24.04	44.31	23.40

Figure 4.5: SEM micrographs and corresponding EDS of (a) carbon deposited region; (b) area of less deposition of carbon; (c) globular structure containing carbon filaments and (d) surface showing formation of pits on metal dusted coupon exposed at 500°C for 300 h.

Exposure at 600°C

Figure 4.6 a shows SEM micrograph of the metal dusted coupon exposed at 600°C for 300 h. The oxide layer formed was uniform and no cracks/ pores were observed. Higher magnification SEM micrograph of the oxide layer shows small crystals embedded in the oxide layer (**Figure 4.6 b**). EDS analysis (spot A) of these crystals shows a high fraction of manganese with oxygen and a small fraction of C and Fe. Similar results were observed by EDS analysis of the rest of the scale (Spot B), in line with the XRD analysis.

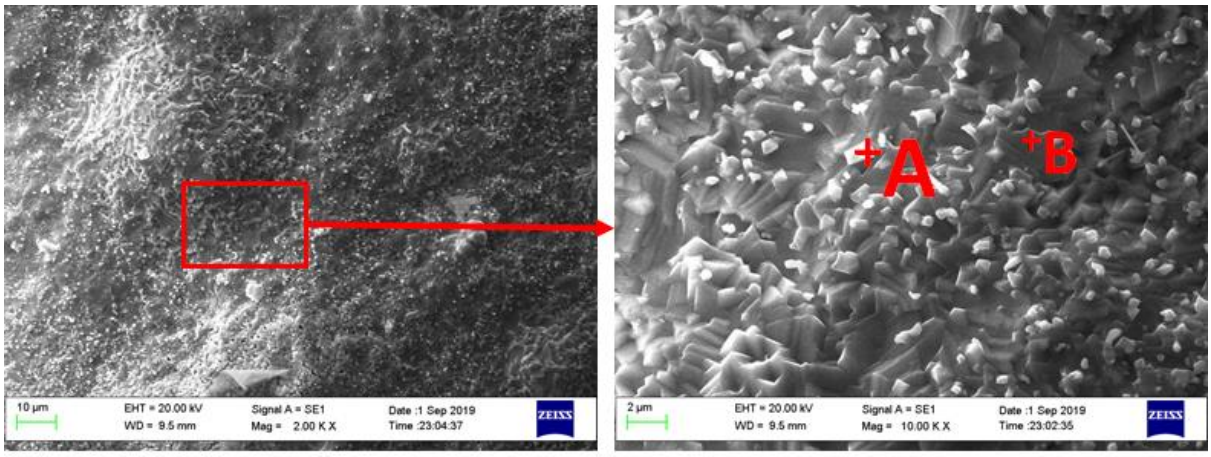

Position	C (wt%)	Fe (wt%)	Mn (wt%)	Cr (wt%)	O (wt%)
A	8.61	2.3	60.74	-	28.35
B	7.03	4.5	61.03	1.4	26.04

Figure 4.6: SEM micrographs and corresponding EDS of (a) oxide layer formed at the surface, (b) magnified image of the selected area (red rectangle) showing crystal formation of metal dusted coupon exposed at 600°C for 300 h.

Exposure at 700°C

Needle-like morphology was observed on metal dusted coupon exposed at 700°C for 300 h (**Figure 4.7 a**). EDS analysis of the needles (spots A and C) shows a higher quantity of manganese and oxygen along with some Fe, Cr, and C. Area elemental analysis also showed similar results (**Figure 4.7 b**). This indicates that there was also some carbon deposition even at 700°C. The high amount of manganese and oxygen in the scale shows formation of MnO in line with the XRD analysis.

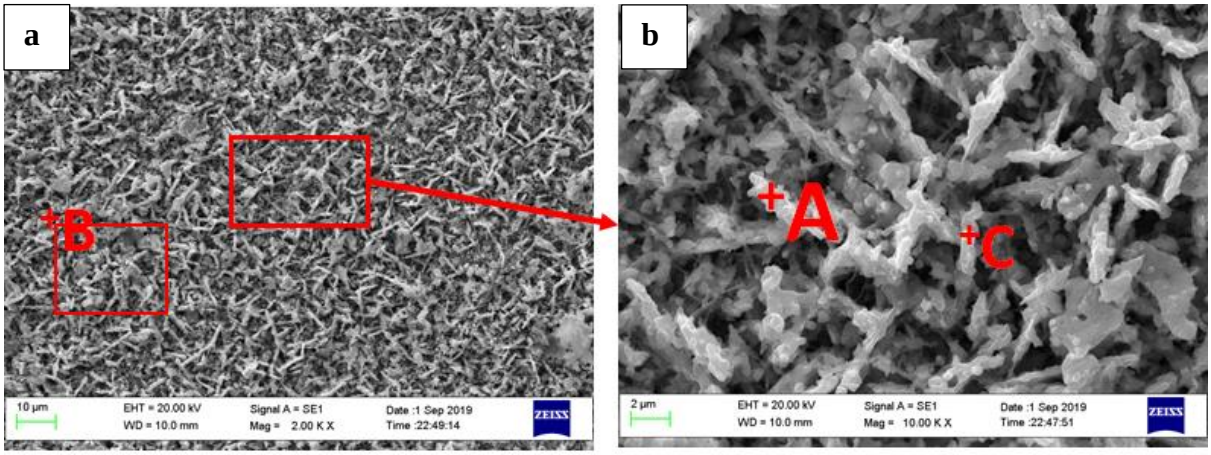

Position	C (wt%)	Fe (wt%)	Mn (wt%)	Cr (wt%)	O (wt%)
A	8.85	9.28	47.26	8.58	26.33
B	11.44	8.34	48.74	8.38	23.1
C	9.5	6.75	46.78	9.51	27.46

Figure 4.7: SEM micrographs and corresponding EDS of metal dusted coupon exposed at 700°C for 300 h: (a) morphology of oxide layer formed at the surface, (b) magnified image of the selected area (red rectangle) showing needle-like structure formation.

4.2.4 Cross Sectional Analysis

Cross sectional analysis of metal dusted coupons was carried out with and without carbon on the surface.

4.2.4.1 SEM (EDS) Analysis

Exposure at 400°C

Figure 4.8 a shows SEM micrograph of cross section of the metal dusted coupon after 300 h of exposure at 400°C. Dense Forest of carbon filaments can be clearly seen on the top surface. EDS area mapping of carbon filaments shows that carbon is present along with Mn and Fe. High magnification examination of the cross section near the exposed surface showed few very shallow pits of ~ 6-7µm depth (**Figure 4.8 b**). EDS mapping of the spots A, B, C, and D in the vicinity of the pit shows a significant amount of carbon and other matrix elements. **Figure 4.8 b** (spot E) taken away from the pit showed only the matrix elements which means that internal carburization and oxidation were limited up to a depth of 2-7µm from the surface.

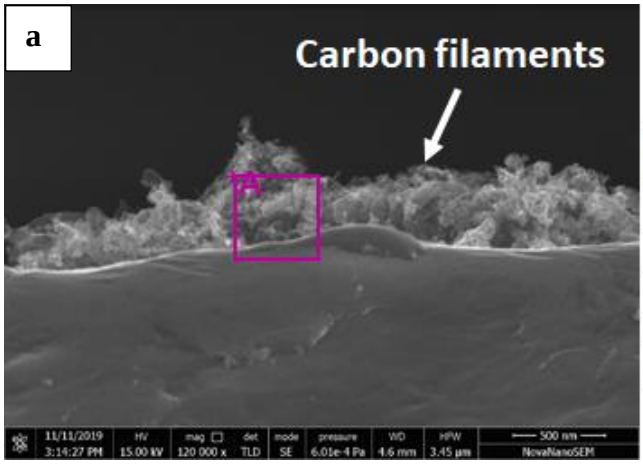

Element	Weight %
C K	44.88
O K	7.38
Cr K	7.05
Mn K	15.41
Fe K	25.29

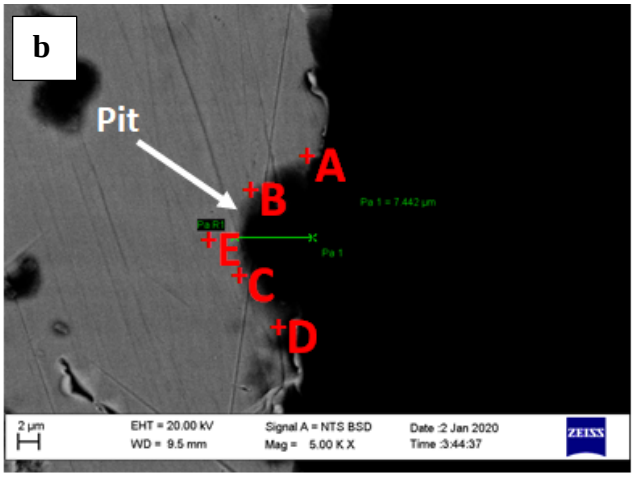

Position	C (wt%)	Cr (wt%)	Mn (wt%)	Fe (wt%)
A	15.28	19.42	21.78	47.22
B	18.12	19.01	19.89	42.98
C	18.23	21.32	20.893	39.52
D	20.17	16.23	21.82	41.78
E	-	19.82	22.3	58.47

Figure 4.8: SEM micrographs and corresponding EDS of (a) cross-section of metal dusted coupon exposed at 400°C for 300 h showing carbon deposition in filament form, (b) BSE micrograph showing pit depth.

Exposure at 500°C

Figures **4.9 a** and **b** shows cross sectional SEM micrographs of the coupon exposed at 500°C before carbon removal. It shows that carbon deposited on the surface is in globular form and had grown in different directions. EDS area mapping of a forest of carbon filaments shows high carbon content and comparatively less manganese than that observed in the sample exposed at 400°C. **Figure 4.9 b** shows cross sectional SEM micrograph in BSE mode, of the pits formed at the surface. The pit size was around ~2-4 µm. EDS point analysis in the vicinity of bottom of the pits (**Figure 4.9 b**, spots A, B, C, and D) showed carbon (>13 wt%) with matrix elements Cr, Mn, and Fe, and no oxygen was observed. This

indicates that metal carbides formed due to internal carburization and caused disintegration of the metal particles. EDS point analysis away from the pits at spot E showed that diffusion of carbon was restricted only to surface up to a depth of 1-2μm.

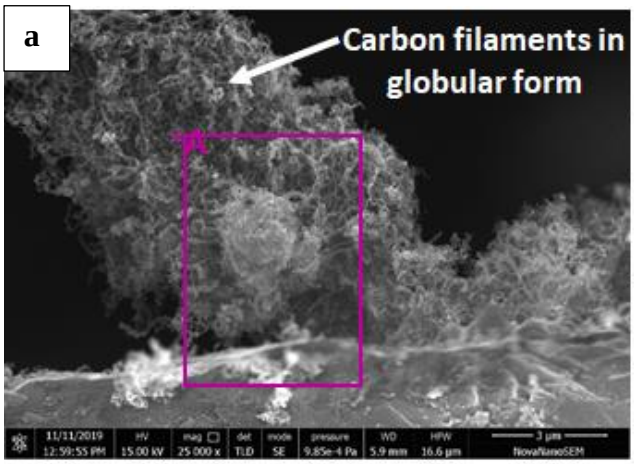

Element	Weight %
C K	66.87
O K	4.65
Cr K	1.61
Mn K	8.26
Fe K	18.61

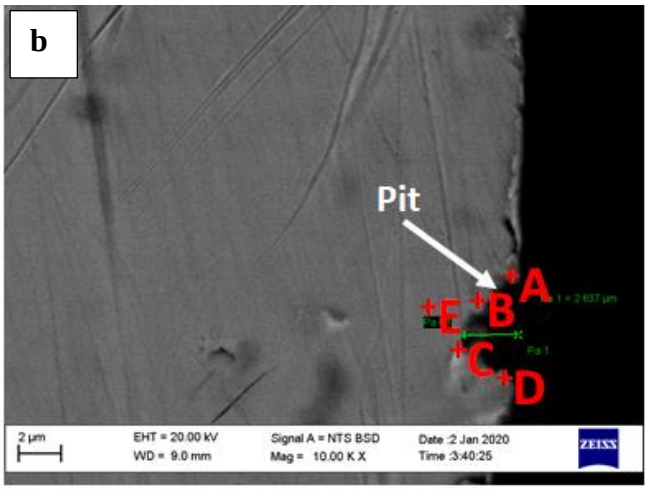

Position	C (wt%)	Cr (wt%)	Mn (wt%)	Fe (wt%)
A	14.35	17.80	20.63	47.22
B	16.67	16.29	19.86	47.18
C	17.73	15.24	17.98	49.05
D	21.11	15.90	19.20	43.79
E	-	19.13	16.53	64.33

Figure 4.9: SEM micrographs and corresponding EDS of (a) cross-section of metal dusted coupon exposed at 500°C for 300 h showing carbon deposition in filament form, (b) BSE micrograph showing pit depth.

Exposure at 600°C

BSE micrograph of metal dusted coupon exposed at 600°C for 300 h clearly shows the distinction between the oxide layer and bulk alloy matrix (**Figure 4.10**). Two different contrasts can be observed in the micrograph, while one is dark grey consisting of MnO (spot A), the other is light grey (spot C) composed of high Mn with Cr and O. The region at the junction of the first and second layers (spot B) contains manganese, chromium,

oxygen, and a little amount of carbon. Pores were also visible in the top dark layer. The oxide thickness was non uniform and varied between 4-7μm. It seems that manganese and chromium got depleted from the matrix and formed Mn, Cr spinel with oxygen. At the interface between the scale and bulk alloy matrix, black regions (spots D and G) were observed. The EDS analysis shows carbon and oxygen with matrix elements Fe and Cr in it. This type of carburization occurs during the initial stages of metal dusting, whereas in later stages selective oxidation of these carbides occurs. Spots E and F are from the matrix which is completely depleted of Mn. The carburization was limited to only surface region up to depth of 1-2μm from the surface.

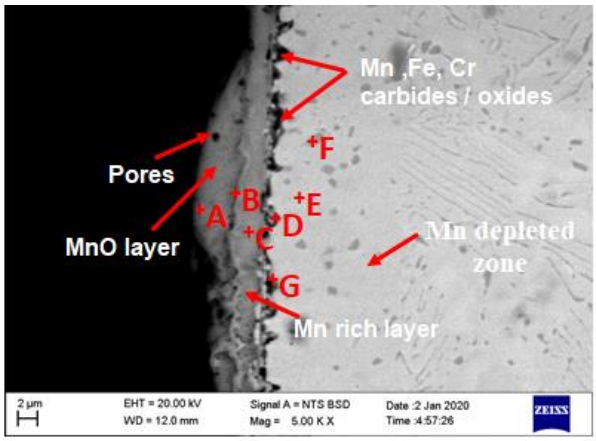

Position	C (wt%)	Fe (wt%)	Mn (wt%)	Cr (wt%)	O (wt%)
A	-	-	73.28	-	26.72
B	18.79	-	40.69	12	28.52
C	-	-	67.78	18.96	13.26
D	15.47	53.30	-	17.73	13.56
E	-	83.69	-	16.31	-
F	-	50.54	-	49.46	-
G	13.3	28.6	14.6	17.5	10.6

Figure 4.10: SEM-BSE micrograph and EDS analysis showing two-layered structure of oxide scale and oxide/carbide region of metal dusted coupon exposed at 600°C for 300 h.

Exposure at 700°C

BSE image of the cross section of the metal dusted coupon exposed at 700°C for 300 h shows two different layers and the matrix (**Figure 4.11**). The top layer of MnO (dark grey) is very thick and porous as compared to that formed at 600°C (spots A and B). The second light grey layer consists of high manganese with chromium and oxygen. At the junction of the first and second layers (spot B), Mn, Cr, O and little amount of carbon was present, similar to that formed at 600°C. At the interface of the scale and alloy matrix, oxygen/carbon was present (spots E, G, and H) along with Fe and Cr, which shows that

oxides and carbides of iron and chromium formed. The oxide layer was non-uniform and the thickness varied between 13-18µm. Spot F corresponds to Mn depleted zone which contains Fe and Cr.

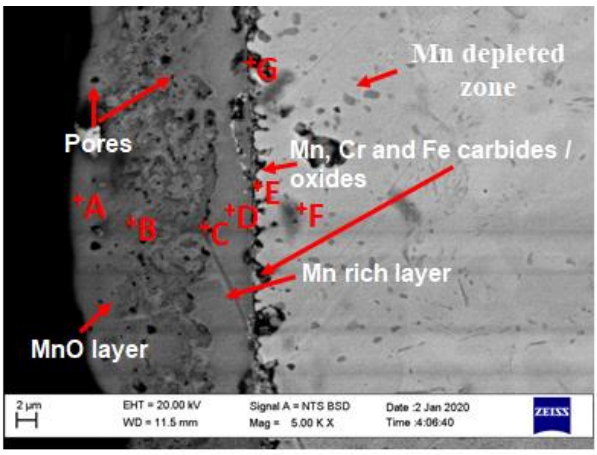

Position	C (wt%)	Fe (wt%)	Mn (wt%)	Cr (wt%)	O (wt%)
A	-	-	67.85	-	31.15
B	-	-	64.83	-	30.17
C	15.64	-	41.96	10.97	31.43
D	-	-	77.30	13.26	9.44
E	16.96	27.65	15.65	26.62	13.54
F	-	58.96	-	41.04	-
G	19.15	22.77	7.50	31.01	18.47

Figure 4.11: SEM-BSE micrograph and EDS analysis showing two-layered structure of oxide scale and oxide/ carbide region in the metal dusted coupon exposed at 700°C for 300 h.

4.2.4.2 EPMA Analysis

Figure 4.12 (a-d) shows EPMA area mapping of Cr, Fe, Mn, and O in cross section of the metal dusted coupons exposed at 400-700°C for 300 h. At 400°C depletion of matrix elements was not observed (**Figure 4.12 a**); however, some content of oxygen was observed at the interface. At 500°C depletion of Mn, Fe, and Cr started but was very much restricted to near the surface (**Figure 4.12 b**). Heavy depletion of Mn from the matrix can be seen at 600°C (**Figure 4.12 c**), while Cr and Fe do not show depletion, instead Fe gets enriched at the surface. A very thin chromium layer can be seen in between the MnO layer which was also confirmed from the EDS analysis (**Figure 4.11**, spot C). Piping structure was observed at the interface enriched with Mn, Cr, and O. It shows formation of spinel of these elements with oxygen. Intensive depletion of Cr and Mn was observed in the metal dusted coupon exposed at 700°C for 300 h and also localized rupture of oxide scale can be seen in **Figure 4.12 d**.

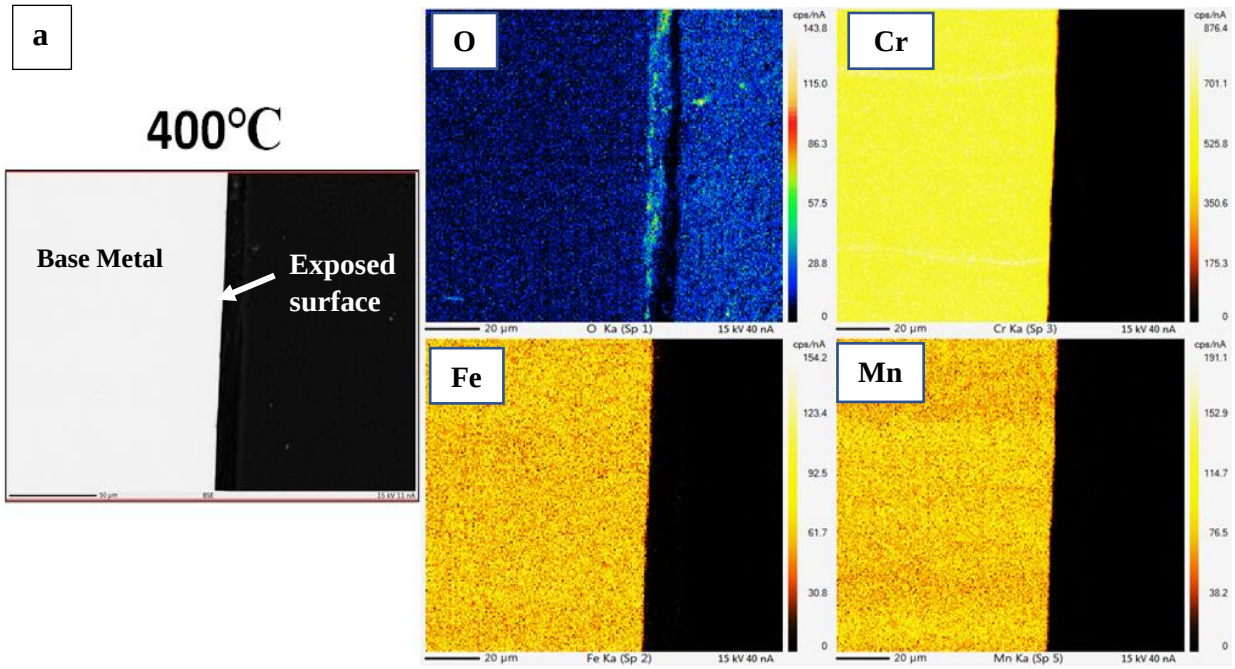
a
400°C
Base Metal
Exposed surface
O
Cr
Fe
Mn
20 µm
O Ka (Sp 1)
Cr Ka (Sp 3)
Fe Ka (Sp 2)
Mn Ka (Sp 5)
15 kV 40 nA

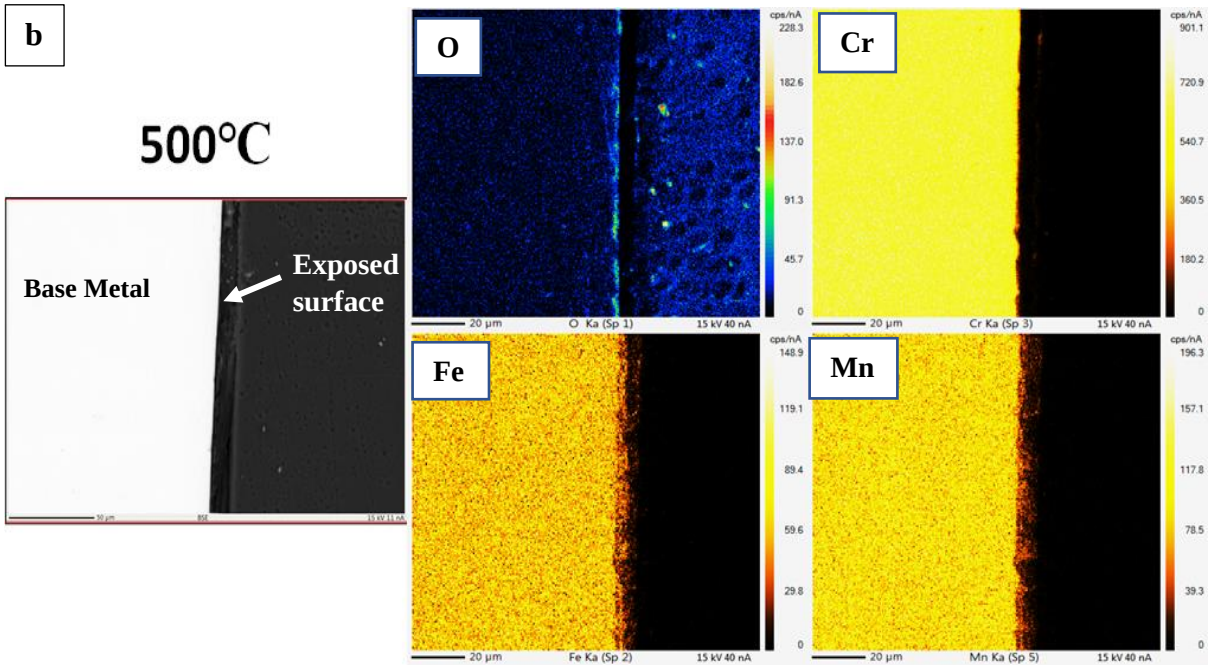
b
500°C
Base Metal
Exposed surface
O
Cr
Fe
Mn
20 µm
O Ka (Sp 1)
Cr Ka (Sp 3)
Fe Ka (Sp 2)
Mn Ka (Sp 5)
15 kV 40 nA

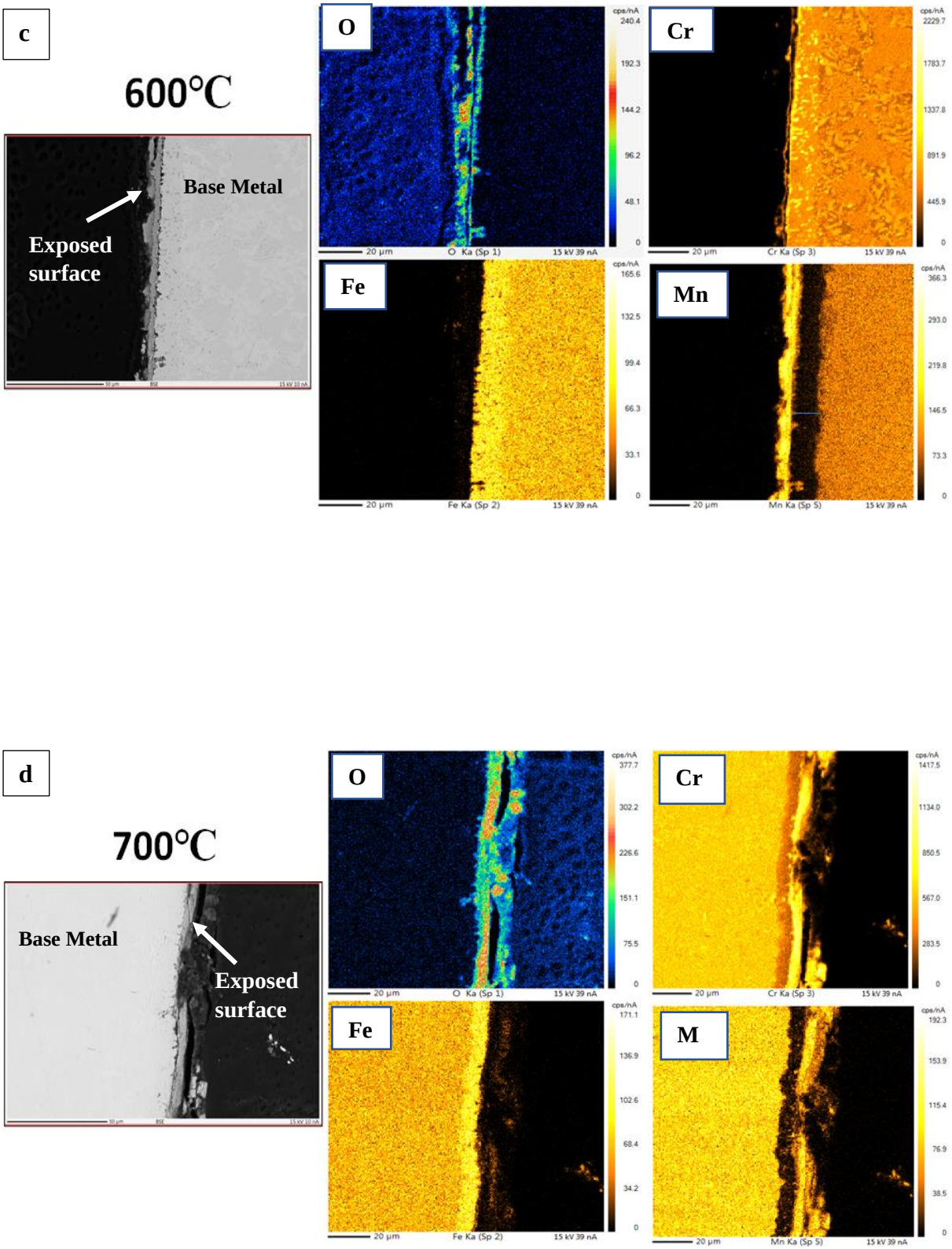

Figure 4.12: EPMA area mapping of metal dusted coupon exposed for 300 h at (a) 400, (b) 500, (c) 600, and (d) 700°C respectively.

Fe gets enriched at the interface which shows that formation of the spinel of Mn-Cr-O restricted the diffusion of carbon into the oxide layer. A distinct region of Cr depletion from the matrix can be seen which is not visible at a lower temperature. MnO layer at the top and then spinel of Cr, Mn, and O at the interface can be seen from Mn, Cr, and O mapping. The same trend was observed at 600°C but the Cr enriched region was very thin while at 700°C it was thick.

4.3. Discussion

The metal dusting features of the low nickel high Mn austenitic stainless steel can be divided into two regimes. Regime I (400-500°C), where the high activity of carbon resulted in filamentous growth of carbon and Regime II (600-700°C), where rapid oxidation of Mn inhibited the growth of carbon filaments. These features are discussed below.

4.3.1 Regime I: Metal Dusting Features at 400-500°C

The metal dusting mechanism of various austenitic stainless-steels containing Ni has been well established and found that Type II and III mechanisms of metal dusting are applicable for such steels [46, 49, 55, 85, 110]. High manganese nitrogen stabilized low nickel containing austenitic stainless steel can be used safely up to the temperature of 500°C for 100 h in ambient air without any danger of precipitation of harmful phases and oxide scaling. Above 500°C, these alloys rapidly form oxide scales and exhibit poor oxidation resistance, forming thick layers of oxides and spinel of Mn, Cr, Fe, and O. Mn has high affinity for oxygen compared to Cr and Fe (Table 4.2), forms stable MnO layer during high temperature exposure. In the present study, under reducing gas atmosphere carbon deposition occurred at 400 and 500°C after long exposure of 300 h. Visual images of the coupons exposed at 400-500°C show that carburization reaction dominated over the oxidation reactions. At 400 and 500°C, significant weight gain was observed due to carbon deposition. Carbon deposition at 400°C was highest (0.39 mg/cm^2) due to higher activity

of carbon and was followed by that at 500°C (0.24 mg/cm^2).

Table 4. 2: Gibbs free energy (kcal/mol K^{-1}) of formation of various carbides and oxides [111, 112].

T(°C)	Cr_2O_3	MnO	Fe_3C	Mn_7C_3	$Cr_{23}C_6$
400	-152.46	-160.46	2.72	-8.11	-14.88
500	-146.50	-156.99	2.09	-7.81	-15.19
600	-142.36	-153.58	1.50	-7.51	-15.49
700	-138.22	-150.03	0.98	-7.21	-15.80

At 400°C diffusion of matrix elements was not prominent as analyzed from EPMA (**Figure 4.12 a**) but SEM/EDS analysis (**Figure 4.8 b**) and XRD patterns show formation of spinel of the $MnCr_2O_4$. Carbon diffusion from the high activity gas mixture to the matrix leads to formation of supersaturated carbides of matrix elements (Mn_7C_3, Fe_3C) as per the following reactions:

$$CO + H_2 + Matrix(Fe, Mn, Cr) \rightarrow \underline{C}(\mathrm{Fe, Mn, Cr}) + \mathrm{H_2}O \quad (4.1)$$

$$23Cr + 6\underline{C} \rightarrow C_{23}C_6 \quad (4.2)$$

$$7Mn + 3\underline{C} \rightarrow Mn_7C_3 \quad (4.3)$$

This results in volume expansion and causes disintegration of matrix into corrosion products containing metal dust, carbon, and few oxides. [51, 110]. Fragmentation of particles leads to formation of localized pit at the surface (**Figures 4.4 e** and **4.5 d**). The growth of carbon filaments starts from the chemically favorable locations at the gas metal interface. The most complete and comprehensive description of the formation mechanism of pits is the carbide cycle mechanism. Decomposition of hydrocarbons occurs in the temperature range of 400-700°C primarily on certain most active ("front") faces of crystals of iron subgroup metals to form intermediate surface carbide like compounds. Decomposition of carbides leads to formation of carbon atoms, which enter a metal particle

and diffuse through it to "rear" faces of metal crystals [60]. Later, carbon is released as nanosized carbon products. The fragmented supersaturated carbides particles (containing >60 wt% carbon) as shown in **Figure 4.4 d** also act as nucleation sites for the growth of carbon filaments at 400°C. The dust particles of metals Fe and Mn diffuses out through these filaments and act as a catalyst for the deposition and growth of carbon (reaction 1.10). Some of the carbides may get oxidized to form oxides and the resulting free carbon further gets diffused into the metal matrix (reactions 4.4-4.6).

$$Mn_7C_3 \rightarrow 7Mn + 3C \quad (4.4)$$

$$2Mn_7C_3 + 7O_2 \rightarrow 14MnO + 6C \quad (4.5)$$

$$Mn_7C_3 + 7O_2 \rightarrow 7MnO_2 + 3C \quad (4.6)$$

MnO shows resistance towards carbon deposition but at lower temperature formation of this layer was not prominent as it is clear from the EPMA analysis (**Figure**s **4.12 a** and **b**). Formation of MnO_2 can be due to oxidation of carbon supersaturated manganese particles by the oxygen liberated through water dissociation (reaction 1.12). At 500°C, the mechanism was similar but the carbon deposited at the surface had different morphology than that at 400°C. Branched filaments morphology was observed at 400°C but at 500°C globular carbon filaments were formed. The exact reason for this kind of behavior could not be explained here and is under investigation.

Spinel of Fe, Mn and oxygen were formed at the surface due to selective oxidation of carbides of Fe and Mn. The depletion of Fe and Mn can be seen from the EPMA analysis. The cross-section morphologies of the coupons exposed at 400-500°C clearly show formation of shallow pits of small sizes. EDS analysis at the bottom of the pits shows that both internal diffusion of carbon along with external growth had occurred simultaneously.

Since the initial chromia layer on the surface of the alloy is hard to penetrate, carbon atoms attack the matrix elements on the most active front very slowly. The defects in the protective chromia layer allow ingress of carbon and the internal carburization under surface causes localized pitting. Rehealing of chromia layer becomes extremely difficult due to formation of stable metal carbides. Based on our above observation, metal dusting mechanism operating at 400 and 500 °C is schematically presented in **Figure 4.13**. Type III mechanism of metal dusting is found applicable for the low nickel high Mn stainless steel. It is interesting to note that nitrogen present in the steel remained inactive during the entire metal dusting process. It has also been reported that nanoparticles present in the oxide scale provide a route for faster transport of carbon through the protective scale [113]. Buyanov et al. [60] have nicely explained the carbon erosion by carbide cycle mechanism. They explained that diffusion transfer of carbon atoms through the metal particle from the 'front' to the 'rear' side causes the most significant perturbations of its structure and properties and also chemical phase separation in the case of alloys. The intense diffusion flow of carbon atoms passes through the particle, which induces strong vibration of the element crystal lattice.

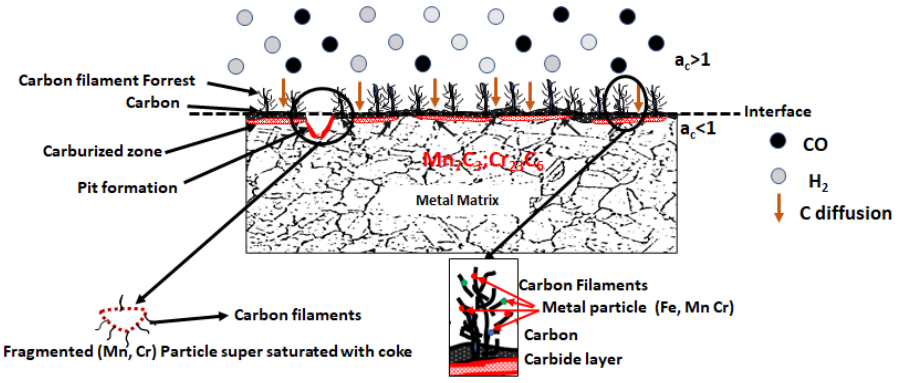

Figure 4.13: Schematic diagram showing mechanism of metal dusting from exposure at 400 and 500°C**.**

This process occurs under the conditions of huge supersaturation of alloying elements with carbon, due to which the system becomes liquid like and experiences viscous flow. The

metal phase in the viscous flow state can enter the lumen of carbon tubes and be carried over with them from the system. The sizes of the metal particles on which nanosized carbon products can form are limited. These sizes depend on the diffusion coefficient of carbon atoms through a metal [61].

4.3.2 Regime II: Metal dusting cum Oxidation at 600-700°C

At 600 and 700°C, the metal dusting mechanism was different, here oxidation of Mn played an important role in preventing filamentous growth of carbon. In other words, the anti-coking property of Mn oxide inhibited carbon erosion. Various studies show that MnO and spinel of $MnCr_2O_4$ exhibit anti coking properties [109, 114]. Mn has the least catalytic properties towards carbon formation compared to Fe, Cr, and Ni [115]. At lower temperatures of 400 and 500°C, MnO layer formation was very limited but as the temperature increased a distinct layer of MnO can be seen from EPMA (**Figure 14 c** and **d**) and SEM-EDS analysis (**Figure 4.10** and **4.11**). MnO layer inhibits deposition of carbon as observed from the SEM micrographs and the carbon weight gain plots. The activity of carbon decreases with an increase in temperature, but was high enough for carbon deposition as reported in the earlier study [85]. Since Mn exhibits multiple valence states, MnO has capability of storing oxygen at very high as well as very low oxygen partial pressure[114]. The oxygen stored in MnO easily dissociates at a very low partial pressure of oxygen in reducing atmosphere. Hence, a small amount of carbon deposition was observed at 600 and 700°C. MnO is highly basic in nature, it enriches the catalyst (Fe) surface with electrons, and promotes steam adsorption at the surface, resulting in suppression of carbon formation [116]. High oxygen storage capacity of MnO leads to oxidation of carbon and soot formation at the surface. During the initial stages, carbon deposition by the reaction 1.10 takes place. Diffusion of carbon in the matrix causes the formation of carbides of Fe and Cr at 600 and 700°C (**Figure**s **4.9** and **4.10**). As time

increases, diffusion of Mn from the matrix starts through the passive chromia layer which combines with the oxygen generated from reaction 1.12 to form oxides. Rapid outward channelized diffusion of Mn generated a distinct Mn depletion zone of ~ 15-20 μm and is visible from the SEM and EPMA studies. Once the MnO layer was formed, carbon deposition was suppressed. Both at 600 and 700°C two layered structure was observed from the SEM-EDS and EPMA analysis of the cross section. At 600°C, the first layer consists of MnO and the second layer of spinel of Mn, Cr and oxygen ($MnCr_2O_4$). Due to outward diffusion of manganese from the matrix, carburized layer shows carbides of Fe and Cr. Similar trend was observed at 700°C. In the present investigation, carbon could not be mapped due to requirement of coating of thin layer of carbon on the polished surface of the coupons for EPMA analysis. A thin chromia layer was observed at 600°C which got thickened at 700°C. Enrichment of Mn in the outer layer was due to its higher binding energy (0.15 eV) with vacancies than that of Cr (0.05 eV) which caused faster diffusion of Mn through the vacancies formed in the chromia layer [101].

Previous studies show that diffusion coefficient of manganese is higher than that of Fe and Cr in the chromia layer. It varies as $D_{Mn}>D_{Fe}>D_{Cr}$ both, through the matrix as well as the chromia layer [102]. Mn oxide also has a lower position than Cr oxide and Fe oxide in the Ellingham-Richardson diagram, which shows that it has the lowest Gibbs free energy of formation and has higher affinity towards oxygen. Diffusion of Mn from the matrix to chromia oxide occurs through grain boundaries and lattice. The effective diffusion through the matrix can be given by Harts equation [98, 99] :

$$D_{eff} = (1-f)D_L + fD_{GB} \quad (4.7)$$

where f is fraction of grain boundaries, D_{GB} is grain boundary diffusion coefficient and D_L is lattice/bulk diffusion coefficient. Generally, grain boundary diffusion is faster than bulk

diffusion. The extent of solute atoms delivered at the metal oxide interface depends on the lattice diffusion [101]. A study carried out by Smith et al. on the self-diffusion coefficient of Mn in 316L shows that for lattice diffusion higher activation energy (240±4kJ mol^{-1}, 750-1200°C) is required compared to grain boundary diffusion (187±18kJ mol^{-1}, 650-1000°C) [117]. On the other hand, Mn diffusion through chromia film has higher activation energy for the grain boundary diffusion (234±8kJ mol^{-1}) than for lattice diffusion (171±40kJ mol^{-1}) in the temperature of 700-1100°C [98]. It suggests that at a lower temperature in metal matrix, grain boundary diffusion will dominate over bulk diffusion, whereas in chromia layer diffusion through bulk will be prominent. At high temperatures of 600 and 700 °C both grain boundary and bulk diffusion play role in diffusion of Mn through metal matrix to oxide metal interface and through chromia layer. The EPMA analysis shows enrichment of Fe and Cr on the surface at 600 and 700°C, in which chromium took part in oxide formation while Fe remained in matrix, although small content of Fe was observed in the oxide layer. Both Mn and Cr have same order of magnitude of grain boundary diffusion coefficient hence both Mn and Cr diffused simultaneously to form $MnCr_2O_4$ which restricted the diffusion of Fe in the oxide layer [99, 118]. Thus, the mechanism operating at 600 to 700°C is initial internal carburization, causing formation of metastable carbides of Fe and Cr, followed by rapid oxidation of Mn leading to development of a thick layer of porous Mn oxide. The localized rupture of the oxide scale also causes direct exposure of surface to carburizing environment. Since carbon diffuses more rapidly into the matrix than oxygen, it causes formation of Fe_3C and $Cr_{23}C_6$ carbides near surface region below the oxide layer [106, 119]. Carbide and oxide formation reactions are given below:

$$3Fe + C \rightarrow Fe_3C \tag{4.8}$$

$$2Mn + O_2 \rightarrow 2MnO \quad (4.9)$$

$$4Cr + 3O_2 \rightarrow 2Cr_2O_3 \quad (4.10)$$

A comparison of Gibbs free energy of carbides and oxides is shown in Table 4.2. For thermodynamically stable carbides, the accepted sequence of formation according to increasing carbon content is $Cr_{23}C_6 < Mn_7C_3 < Fe_3C$. Outward diffusion of Mn and Cr from the bulk and grain boundary occurs simultaneously and leads to formation of their oxides. The difference between free energy of formation of Cr_2O_3 and MnO is small, hence both forms simultaneously. The above mechanism of metal dusting cum oxidation is explained schematically in **Figure 4.14**. Based on the present investigation it can be summarized that the high Mn nitrogen stabilized austenitic stainless steel showed appreciable resistance to metal dusting at all the temperatures from 400-700°C, for the exposure of 300 h, in comparison with other Ni containing austenitic stainless steels, reported in the literature.

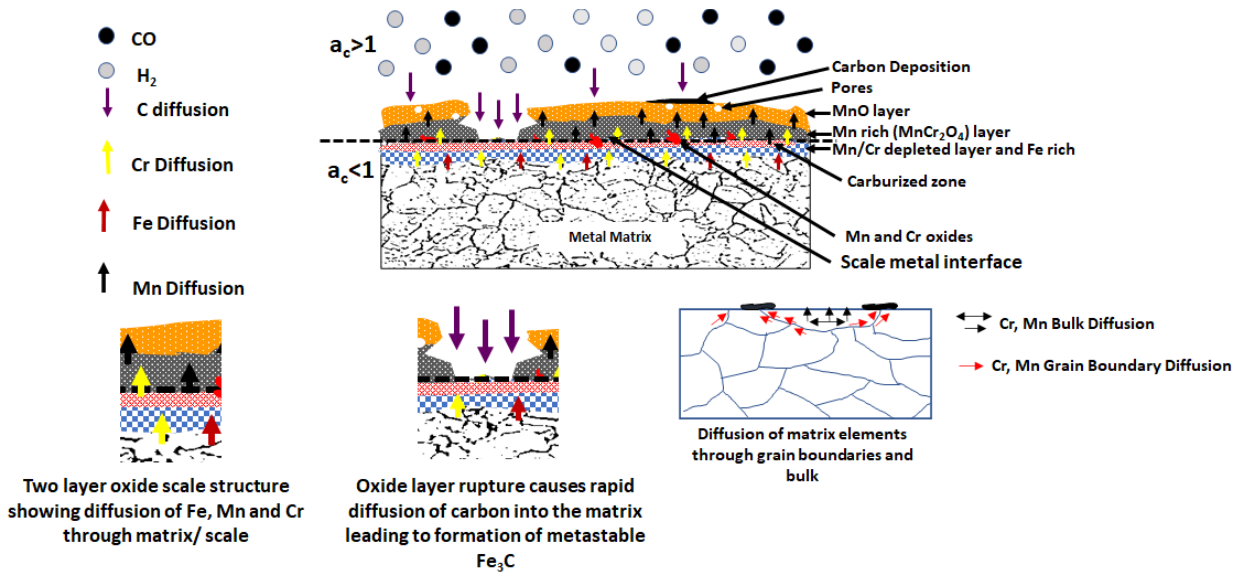

Figure 4.14: Schematic diagram showing the mechanism of metal dusting from exposure at 600 and 700°C.

4.4. Conclusions

Metal dusting features of an extremely low nickel austenitic stainless steel (Fe-18Cr-21Mn-0.65N) was studied in the temperature range of 400-700°C, for 300 h in high carbon activity

(a_c>1) syngas environment (75%H_2+25%CO). Extensive growth of carbon filaments was found from 400-500°C due to high activity of carbon. The limited metal dusting (carbon erosion) of metal particles showed formation of few pits of shallow depth. Metal dust comprising of graphite, Mn, and Fe along with fragmented metal carbide particles formed after low temperature exposure. At high temperature of 600-700°C rapid diffusion of Mn resulted in formation of thick porous layer of Mn oxide which inhibited the growth of carbon filaments. This was followed by an intermediate layer of spinel of Mn, Cr, and O. The presence of few metal carbides/oxides, showed that initially the process started with carburization reaction but later oxidation of these carbides takes place. In short, the alloy exhibited the Type III mechanism of metal dusting where initially formed metastable carbides were selectively oxidized depending upon the activity of carbon.